Semiautomated Building Facade Footprint Extraction From Mobile LiDAR Point Clouds

Bisheng Yang, Zheng Wei, Qingquan Li, and Jonathan Li

***Abstract*—This letter presents a novel method for automated footprint extraction of building facades from mobile LiDAR point clouds. The proposed method first generates the georeferenced feature image of a mobile LiDAR point cloud and then uses image segmentation to extract contour areas which contain facade points of buildings, points of trees, and points of other objects in the georeferenced feature image. After all the points in each contour area are extracted, a classification based on principal component analysis (PCA) method is adopted to identify building objects from point clouds extracted in contour areas. Then, all the points in a building object are segmented into different planes using the random sample consensus algorithm. For each building, points in facade planes are chosen to calculate the direction, the start point, and the end point of the facade footprints using PCA. Finally, footprints of different facades of building are refined, harmonized, and joined. Two data sets of downtown areas and one data set of a residential area captured by Optech's LYNX mobile mapping system were tested to verify the validities of the proposed method. Experimental results show that the proposed method provides a promising and valid solution for automatically extracting building facade footprints from mobile LiDAR point clouds.**

***Index Terms*—Building facades, footprint extraction, mobile LiDAR.**

I. Introduction

AUTOMATIC building extraction and 3-D reconstruction in urban areas have recently been a hot topic in the field of photogrammetry and computer vision. The need for detailed 3-D information about buildings continues to increase steadily. Generally, 2-D outlines or footprints of buildings must be extracted before a volumetric building representation can be constructed. The extracted building footprints constitute an invaluable data source for map updating, 3-D reconstruction, and change detection. Many efforts have been made to address this problem, for instance, by integrating multiple data sources including remote-sensing images [1]–[4] and airborne, mobile, and terrestrial LiDAR data [5], [6] for building footprint extraction.

Manuscript received August 8, 2012; accepted September 28, 2012. This work was supported in part by the National Basic Research Program of China under Grant 2012CB725301, by the National Science Foundation of China project under Grant 41071268, by the project from State Key Laboratory of Resources and Environmental Information Systems, Chinese Academy of Sciences, under Grant 2010KF0001SA, and by the Fundamental Research Funds for the Central Universities under Grant 3103005.

B. Yang, Z. Wei, and Q. Li are with the State Key Laboratory of Information Engineering in Surveying, Mapping, and Remote Sensing, Wuhan University, Wuhan 430079, China.

J. Li is with the Department of Geography and Environmental Management, Faculty of Environment, University of Waterloo, Waterloo, ON N2L 3G1, Canada.

Color versions of one or more of the figures in this paper are available online at http://ieeexplore.ieee.org.

Digital Object Identifier 10.1109/LGRS.2012.2222342

In recent years, airborne LiDAR data have been widely used to extract building footprints or outlines [7]–[9]. The methods for extracting building footprints from airborne LiDAR data usually consist of two steps: coarse footprint extraction and footprint refinement. Other methods include an object-based strategy for extraction of building footprints [10], [11]. However, this method is very time consuming.

To extract building footprints from mobile or terrestrial LiDAR data, vertical walls or facade surfaces are first extracted to represent the building footprints. Hammoudi *et al.* [12], [13] presented an approach for automatic extraction of building footprints and planar clusters of street facades using mobile LiDAR data in urban environment. This approach works well for extracting facade outlines. However, it may have difficulties in individualizing aligned and joined street facades (i.e., coplanar dwelling facades) without prior knowledge. Rutzinger *et al.* [14] combined mobile and airborne LiDAR data to extract vertical walls automatically to form building footprints, using region-growing segmentation. This method requires the 3-D Hough transform for finding the seed surface for region growing, which is a drawback when dealing with mobile LiDAR data over large areas.

Unlike airborne LiDAR data, mobile and terrestrial LiDAR data provide much more detailed information about building facades, which leads to great potential for footprint extraction and building reconstruction at the street level. Although [14] presented a preliminary analysis of the automated extraction of building walls from mobile LiDAR data, approaches for efficiently extracting building footprints from mobile LiDAR data still need to be developed. On the one hand, huge data volumes, redundancy, and occlusion affect the efficiency and potential for automation of mobile LiDAR data processing. On the other hand, the nonuniqueness of the correspondence between the (X, Y)-coordinates and the Z-coordinates of points makes it difficult to extract objects without ancillary information such as scan lines or imagery.

This letter proposes a coarse-to-fine approach which automatically and effectively extracts building facades from mobile LiDAR point clouds in urban environment. The proposed method involves generation of georeferenced feature images of mobile LiDAR point clouds, image processing of the generated georeferenced feature images, identification of building objects, coarse extraction of facades, and refinement of these facades. Fig. 1 elaborates the framework of the proposed method.

II. Generating Georeferenced Feature Images From Mobile LiDAR Data

It is fairly difficult to extract building footprints directly from mobile LiDAR point clouds because of noise (e.g., flying

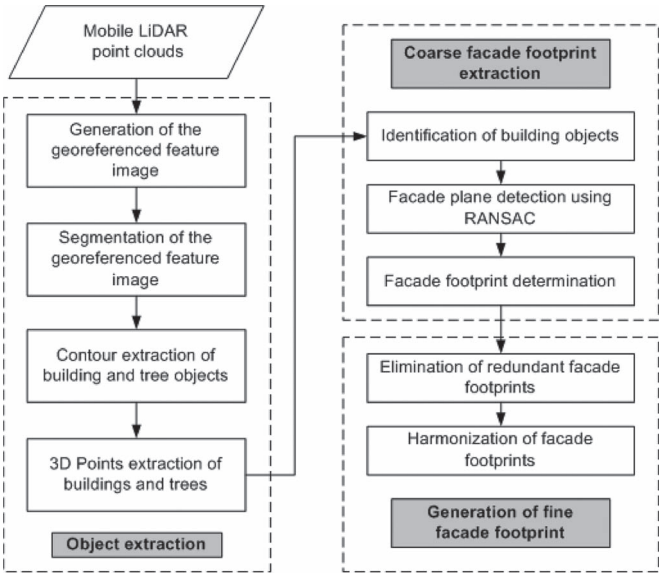

Fig. 1. Framework of the proposed method.

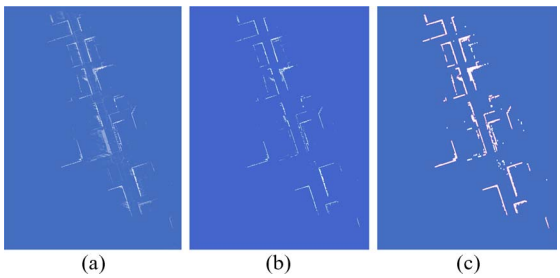

Fig. 2. Segmentation and contour extraction of a georeferenced feature image. (a) Original image. (b) Segmented image. (c) Extracted contours.

bird point) in the data, the huge volume of the data, and the absence of explicit or ancillary data (e.g., image intensities). Yang *et al.* [15] present a method for automated extraction of street-scene objects from mobile LiDAR point clouds. The proposed method first generates the georeferenced feature image of mobile LiDAR point clouds and then extracts the boundaries of street-scene objects (e.g., buildings) by applying the method of image segmentation and contour tracing on the georeferenced feature image generated. Yang *et al.* [15] also provided a comprehensive discussion of parameter selection for generation of georeferenced feature images for different purposes (e.g., building extraction and power-line extraction). The method proposed in [15] was adopted to generate a georeferenced feature image of mobile LiDAR point clouds. Fig. 2(a) shows a georeferenced feature image generated by the method in [15].

A. Segmentation of the Georeferenced Feature Image

In the generated georeferenced feature image, points of greater height have larger gray values. This means that areas with buildings and trees have larger gray values than other areas like roads. To determine two pixel classes from the generated georeferenced feature image, discrete discriminant analysis [16] was used to determine the gray-value threshold automatically because of its robustness. Fig. 2(b) shows a classification result by discrete discriminant analysis.

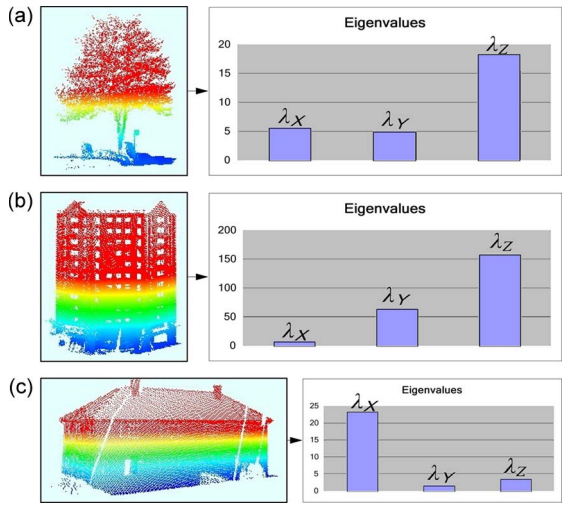

Fig. 3. Different objects and the corresponding eigenvalues. (a) Tree and its eigenvalues. (b) Multistorey building and its eigenvalues. (c) Residential building and its eigenvalues.

B. Contour Extraction of Man-Made Objects

To preserve the completeness of object boundaries, a binary morphological dilation using a (e.g., 2×2, or 3×3, or 5×5) square structuring element is first performed on the segmented feature image. Because this work involves a segmented binary feature image (the background is black), contour extraction is carried out in a simple way. A pixel is changed to white if it is a black pixel, and its eight neighbor pixels are black as well. In this way, black pixels whose eight neighbor pixels are not all black will be labeled as boundary pixels. To trace contours, the contour-tracing algorithm proposed in [17] was used to identify each contour as a sequence of edge points. Fig. 2(c) shows the result of contour extraction of man-made objects in the segmented feature image.

III. Coarse Facade Footprint Extraction

Once the contours of man-made objects have been extracted, the spatial extent of each object can easily be calculated. Then, the point clouds corresponding to each object can be extracted from the mobile LiDAR point clouds according to the spatial extent calculated. As the extracted objects from contours could be buildings or trees, the building objects should first be isolated for extracting facade footprints.

A. Identification of Building Objects

It is difficult to directly distinguish between buildings and trees by gray values in the segmented georeferenced feature image. However, points of buildings and trees show notable differences on spatial distributions in 3-D space. Generally, points of a tree have more obvious distribution in Z-direction than X- or Y-direction [Fig. 3(a)]. However, this characteristic of points may not be applied to buildings because of the different height of buildings in downtown area and buildings in residential area. There is a great disparity between the heights of a multistorey building and of a tree [Fig. 3(b)]. For a residential building, the obvious distribution represents on X- or Y-direction rather than Z-direction [Fig. 3(c)]. Also, the mean area of the profiles in the Z-direction of a tree is usually

much smaller than that of a building. Hence, the eigenvalue analysis based on the PCA method and the profile analysis in Z-direction of the man-made object points are jointly performed to identify the two classes of building objects, i.e., multistorey building and residential building.

To calculate the eigenvalues of an object, the X-, Y-, and Z-coordinates of points belonging to an object are used to construct a covariance matrix $C(3^*3)$, which is calculated by

$$C = \sum_{i=1}^{n} (P_i - P_{\text{center}})^T \times (P_i - P_{\text{center}}) \tag{1}$$

where n is the number of points of the object and the $P_i (1 < i < n)$ denotes the points belonging to the object. P_{center} $(X_{P_{\text{center}}}, Y_{P_{\text{center}}}, Z_{P_{\text{center}}})$ is the 3-D center point of the object points $\{P_i\}$, which is calculated by

$$X_{P_{\text{center}}} = \frac{1}{n}\sum_{i=1}^{n} X_{P_i} \quad Y_{P_{\text{center}}} = \frac{1}{n}\sum_{i=1}^{n} Y_{P_i}$$

$$Z_{P_{\text{center}}} = \frac{1}{n}\sum_{i=1}^{n} Z_{P_i}. \tag{2}$$

The corresponding eigenvalues $(\lambda_X, \lambda_Y,$ and $\lambda_Z)$ of the covariance matrix C can then be calculated (as shown in Fig. 3). According to PCA theory, the three eigenvalues correspond to the characteristics of the whole points in X-, Y-, and Z-directions, respectively.

Generally, the perimeter of tree crown is larger compared with that of tree trunk. The perimeters of building at different heights usually remain at a constant value. In addition, the mean perimeter of a building at Z-direction is usually much larger than that of a tree. Hence, buildings and trees show different profiles at Z-direction. Given an unknown object with points, the area of a profile at a specified height (A_{pi}) can be calculated with all the points lying in the profile at Z-direction. These areas of profiles at different heights are used to compute the mean value (μ_A) of profile areas at Z-direction, which is calculated by

$$\mu_A = \sum_{i=1}^{N_p} A_{pi}/N_p \tag{3}$$

where N_p is the number of profiles of the object at Z-direction. Therefore, a threshold of μ_A can be set to distinguish buildings and trees. Hence, the following rules are defined for classifying building and tree objects by integrating profile analysis in Z-direction and eigenvalue comparison:

Trees :

$(\lambda_Z = \max(\lambda_X, \lambda_Y, \lambda_Z))$

$(\lambda_Z - \min(\lambda_X, \lambda_Y, \lambda_Z) < T_H)$ and $(\mu_A < T_A)$

Multistorey buildings :

$(\lambda_Z = \max(\lambda_X, \lambda_Y, \lambda_Z))$

$(\lambda_Z - \min(\lambda_X, \lambda_Y, \lambda_Z) > T_H)$ and $(\mu_A > T_A)$

Residential buildings :

$(\lambda_X = \max(\lambda_X, \lambda_Y, \lambda_Z))$ and $(\mu_A > T_A)$

or $(\lambda_Y = \max(\lambda_X, \lambda_Y, \lambda_Z))$ and $(\mu_A > T_A)$

where T_H is the threshold of the difference between the maximum eigenvalue and the minimum eigenvalue and T_A is the threshold of the mean value (μ_A) of profile areas in Z-direction. For instance, if the eigenvalue λ_Z of an object is the highest value of $(\lambda_X, \lambda_Y, \lambda_Z)$, λ_Z and μ_A meet the aforementioned conditions of T_H and T_A in the meantime; the object is a multistorey building.

B. Facade Plane Detection of Building Objects

Given a threshold (T_{num}) on the minimum number of points and a normal direction for each facade, the facades of a building can be detected using the RANSAC algorithm [18]. For each detected facade plane, the points with distances to the facade plane less than a specified threshold $d_{\max}$ will be classified into it. Once the points belonging to each facade plane have been determined, the direction, start point, and end point of the facade footprint can be calculated.

C. Facade Footprint Determination Using PCA

To calculate the direction of the detected facade, the X- and Y-coordinates of points belonging to a facade are used to construct a covariance matrix C_1 (2^*2), which can be calculated as follows:

$$C_1 = \sum_{i=1}^{n} (Q_i - Q_{\text{center}})^T \times (Q_i - Q_{\text{center}}) \tag{4}$$

where n is the number of points in the facade and the Q_i $(1 < i < n)$ denotes the points belonging to the facade. Q_{center} $(X_{Q_{\text{center}}}, Y_{Q_{\text{center}}})$ is the 2-D center point of the facade points $\{Q_i\}$, which is calculated by

$$X_{Q_{\text{center}}} = \frac{1}{n}\sum_{i=1}^{n} X_{Q_i} \quad Y_{Q_{\text{center}}} = \frac{1}{n}\sum_{i=1}^{n} Y_{Q_i}. \tag{5}$$

The corresponding eigenvalues (λ_1 and λ_2) and eigenvectors (V_1 and V_2) of the covariance matrix C_1 can then be calculated. The eigenvector V_d corresponding to the larger eigenvalue is the direction of the facade footprint according to PCA theory.

Because Q_{center} has been determined, the 2-D distances between Q_{center} and the points located at the left and right sides of Q_{center} can be calculated. The points on the left and right sides of Q_{center} with the maximum distance to Q_{center} will be identified as the start and end points of the facade footprint. The Z-coordinates of the start and the end points are assigned by the lowest Z-coordinate of points in the facade plane. Once the direction, the start point, and the end point of the facade footprint have been determined, the coarse facade footprint can be obtained.

IV. Refinement and Harmonization of Building Facade Footprints

On the one hand, the RANSAC-based facade extraction method may lead to redundant facades because of the thresholds of T_{num} and $d_{\max}$. Due to the mathematical principle of the

RANSAC algorithm [18], the detected plane varies with the thresholds of T_{num} and $d_{\max}$. On the other hand, complex protrusions or ornaments on building facades can also lead to redundant footprints for a single facade. Hence, it is necessary to eliminate redundant footprints before refining the extracted facade footprints.

A. Elimination of Redundant Facade Footprints

To eliminate redundant facade footprints, the extracted footprints for each building are first classified into different groups using a search of neighboring regions. This search first generates a buffer with a certain width (e.g., three pixels) for the footprint of each building. Suppose that one footprint falls in the buffer area of another footprint. Moreover, suppose that the difference between the slopes of the two footprints is less than a threshold (e.g., 5°). These two footprints are then classified into a single group. Using this search of neighboring regions, all the extracted footprints can be classified into groups. Suppose that a group contains more than one footprint. The redundant footprints should then be removed. To remove redundant footprints, the length and slope of each footprint in the classification group G_j are calculated. Second, the main direction of classification group G_j, which is the average slope of the footprints in the group, is calculated. The footprint with the maximum length and the minimum angle between the footprint and the main direction is kept, and the other footprints are removed. Thus, the footprints for different facades can be obtained after redundant footprints have been removed.

B. Harmonization of Building Facade Footprints

The extracted facade footprints of one building may be disjoint because of occlusion or incomplete extraction. The facade footprints of a single building should be connected to each other. To connect disjoint footprints, a virtual intersection vertex is generated according to the interrelationships among the footprints of the building. The extracted footprints can thus be connected and harmonized.

V. Results

Three data sets of downtown and residential areas captured by the LYNX mobile mapping system were selected to verify the validities of the proposed method. The spatial span of the captured point clouds is approximately 1–5 cm. The numbers of points in data sets *testdata-1*, *testdata-2*, and *testdata-3* are 8 318 968, 10 447 105, and 8 139 726, respectively. The spatial extents of the data sets are approximately 410 m * 560 m, 550 m * 750 m, and 400 m * 350 m, respectively. Fig. 4 shows an overview of *testdata-1*, *testdata-2*, and *testdata-3*.

A. Identification of Building Objects

There are 30, 35, and 53 man-made object contours extracted in the three data sets, respectively. To identify building objects, the points located in each contour extracted were analyzed according to eigenvalue analysis and profile analysis in Z-direction described in Section III-A. In our study, the thresholds of the parameters of T_H and T_A were specified as 30.0 and 20.0, respectively. The building identification results of the three data sets are listed in Table I.

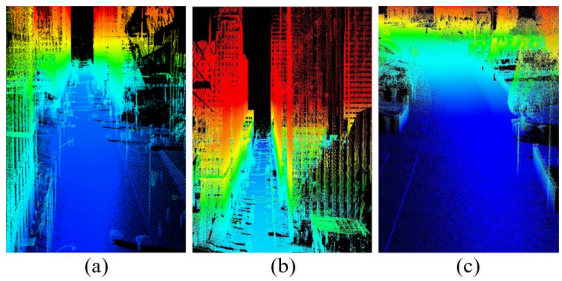

Fig. 4. Overview of the three data sets. (a) *Testdata-1*. (b) *Testdata-2*. (c) *Testdata-3*.

TABLE I
Results of Building Identification for the Three Data Sets

	The number of ground-truth objects			Identification result of buildings and trees		
	multi-storey buildings	residential buildings	trees	multi-storey buildings	residential buildings	trees
Testdata-1	30	0	0	30	0	0
Testdata-2	34	1	0	34	1	0
Testdata-3	0	50	3	0	52	1

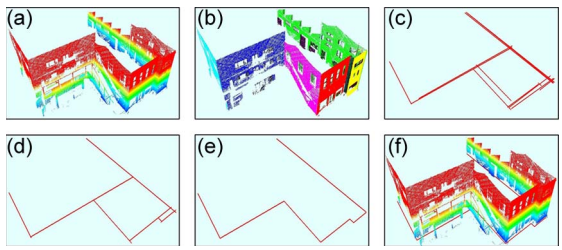

Fig. 5. Facade footprint extraction of a complex building. (a) Point cloud of the building. (b) Facade segmentation result. (c) Coarse level of footprints. (d) Eliminating redundant footprints. (e) Refining footprints. (f) Matching extracted footprints.

B. Facade Footprint Extraction Results

Fig. 5 shows the procedure of facade footprint extraction of a complicated building. It can be seen that the building has complex facades with obvious protrusions. Fig. 5(a) and (b) shows the extracted points and facades, respectively. The extracted facades were dotted with different colors. It can be seen that the RANSAC method works properly. As shown in Fig. 5(b), redundant facade planes were detected which led to redundant footprints as shown in Fig. 5(c). On the other hand, it can be seen from Fig. 5(c)–(e) that the method described in Section IV correctly extracted the coarser footprints and refined the extracted footprints properly. This was demonstrated by matching the refined footprints with the original points as shown in Fig. 5(f). Fig. 6 shows the refined building facade footprints extracted from *testdata-3*.

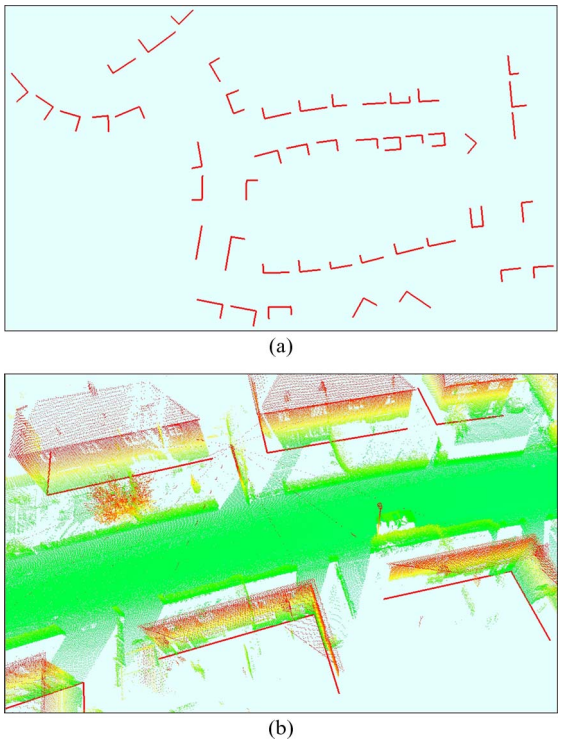

Fig. 6. Extraction of facade footprints for *testdata-3*. (a) Refined footprints. (b) Matching extracted facade footprints and original point clouds.

VI. Conclusion

Automated extraction of meaningful features from mobile LiDAR data is still a challenging task, although extensive efforts have been made in this area. Compared with the capture of mobile LiDAR data, which is straightforward, the processing of these data urgently requires powerful and effective solutions for purposes such as emergency mapping, feature extraction, data fusion, and 3-D reconstruction. This letter has proposed an automated method for extracting building facade footprints from mobile LiDAR data. The proposed method first generates a georeferenced feature image from the mobile LiDAR data, thus transforming the problem of understanding point clouds into that of understanding images. Then, the method uses image processing, the RANSAC algorithm, and PCA to extract coarse facade footprints. Finally, the extracted facade footprints are refined using the interrelationships of the footprints belonging to each building. Three data sets captured by the LYNX mobile mapping system were selected to verify the validities of the proposed method. The results achieved appear encouraging and demonstrate that the proposed method provides an effective solution for extracting building facade footprints from mobile LiDAR data. The extracted facade footprints are not only beneficial for facade reconstruction but are also meaningful for the segmentation of building point clouds. Moreover, the proposed method provides a new solution for mapping and understanding mobile LiDAR point clouds.

Some issues remain to be addressed in future research. Reflection intensities of point clouds and associated imagery will be incorporated for better point-cloud mapping and understanding, which will improve the extraction of facade footprints. The footprint extraction of buildings which have cylindrical facades and even more complex structures still needs further study.

Acknowledgment

The authors would like to thank Optech Inc. for providing the data sets.

References

[1] L. Sahar, S. Muthukumar, and S. P. French, "Using aerial imagery and GIS in automated building footprint extraction and shape recognition for earthquake risk assessment of urban inventories," *IEEE Trans. Geosci. Remote Sens.*, vol. 48, no. 9, pp. 3511–3520, Sep. 2010.

[2] H. Akçay and S. Aksoy, "Automatic detection of geospatial objects using multiple hierarchical segmentations," *IEEE Trans. Geosci. Remote Sens.*, vol. 46, no. 7, pp. 2097–2111, Jul. 2008.

[3] H. Mayer, "Automatic object extraction from aerial imagery—A survey focusing on buildings," *Comput. Vis. Image Understand.*, vol. 74, no. 2, pp. 138–149, May 1999.

[4] S. Ahmadi, M. J. Valadan Zoej, H. Ebadi, H. A. Moghaddam, and A. Mohammadzadeh, "Automatic urban building boundary extraction from high resolution aerial images using an innovative model of active contours," *Int. J. Appl. Earth Observ. Geoinf.*, vol. 12, no. 3, pp. 150–157, Jun. 2010.

[5] L. Matikainen, J. Hyyppä, and H. Hyyppä, "Automatic detection of buildings from laser scanner data for map updating," *Proc. Int. Arch. Photogramm. Remote Sens. Spatial Inf. Sci.*, vol. 35, pp. 218–224, 2003.

[6] G. Vosselman, B. G. H. Gorte, and G. Sithole, "Change detection for updating medium scale maps using laser altimetry," in *Proc. Int. Arch. Photogramm., Remote Sens. Spatial Inf. Sci.*, 2004, vol. 34, pp. 207–212.

[7] G. Sohn and I. Dowman, "Data fusion of high-resolution satellite imagery and LiDAR data for automatic building extraction," *ISPRS J. Photogramm. Remote Sens.*, vol. 62, no. 1, pp. 43–63, May 2007.

[8] O. Wang, S. K. Lodha, and D. P. Helmbold, "A Bayesian approach to building footprint extraction from aerial LiDAR data," in *Proc. Int. Symp. 3D Data Process., Vis., Transmiss.*, 2006, pp. 192–199.

[9] K. Zhang, J. Yan, and S. C. Chen, "Automatic construction of building footprints from airborne LiDAR data," *IEEE Trans. Geosci. Remote Sens.*, vol. 44, no. 9, pp. 2523–2533, Sep. 2006.

[10] E. A. S. Galvanin and A. P. Dal Poz, "Extraction of building roof contours from LiDAR data using a Markov-random-field-based approach," *IEEE Trans. Geosci. Remote Sens.*, vol. 49, no. 3, pp. 981–987, Mar. 2012.

[11] O. Tournaire, M. Brédif, D. Boldo, and M. Durupt, "An efficient stochastic approach for building footprint extraction from digital elevation models," *ISPRS J. Photogramm. Remote Sens.*, vol. 65, no. 4, pp. 317–327, Jul. 2010.

[12] K. Hammoudi, F. Dornaika, B. Soheilian, and N. Paparoditis, "Extracting outlined planar clusters of street facades from 3D point clouds," in *Proc. Can. Conf. Comput. Robot Vis.*, 2010, pp. 122–129.

[13] K. Hammoudi, F. Dornaika, B. Soheilian, and N. Paparoditis, "Extracting wire-frame models of street facades from 3D point clouds and the corresponding cadastral map," in *Proc. Int. Arch. Photogramm., Remote Sens. Spatial Inf. Sci.*, 2010, vol. 38, pp. 91–96.

[14] M. Rutzinger, S. Oude Elberink, S. Pu, and G. Vosselman, "Automatic extraction of vertical walls from mobile and airborne laser scanning data," in *Proc. ISPRS/LASER*, 2009, vol. 38, pp. 7–11.

[15] B. S. Yang, Z. Wei, Q. Q. Li, and J. Li, "Automated extraction of street-scene objects from mobile LiDAR point clouds," *Int. J. Remote Sens.*, vol. 33, no. 18, pp. 5839–5861, Sep. 2012.

[16] M. Goldstein and W. R. Dillon, *Discrete Discriminant Analysis*. New York: Wiley, 1978.

[17] T. Pavlidis, *Algorithms for Graphics and Image Processing*. Rockville, MD: Computer Science, 1982.

[18] F. Tarsha-Kurdi, T. Landes, and P. Grussenmeyer, "Hough-transform and extended RANSAC algorithms for automatic detection of 3D building roof planes from Lidar data," in *Proc. Int. Arch. Photogramm., Remote Sens. Spatial Inf. Sci.*, 2007, vol. 36, pp. 407–412.